Chemosphere 303 (2022) 134947

Contents lists available at ScienceDirect

Chemosphere

journal homepage: www.elsevier.com/locate/chemosphere

Polystyrene micro and nano-particles induce metabolic rewiring in normal human colon cells: A risk factor for human health

Marcella Bonanomi [a,b], Noemi Salmistraro [a,c], Danilo Porro [a,c], Annalisa Pinsino [d], Anna Maria Colangelo [a,b], Daniela Gaglio [a,c,*]

[a] ISBE. IT/ Centre of Systems Biology, Piazza Della Scienza 4, 20126, Milan, Italy
[b] Department of Biotechnology and Biosciences, University of Milano-Bicocca, Piazza Della Scienza 2, 20126, Milan, Italy
[c] Institute of Molecular Bioimaging and Physiology (IBFM), National Research Council (CNR), Segrate, MI, Italy
[d] Institute of Translational Pharmacology (IFT), National Research Council (CNR), Palermo, PA, Italy

HIGHLIGHTS

- Acute and chronic NPs and MPs exposure cause metabolic rewiring and oxidative stress.
- Chronic NPs or MPs exposure induces decoupling of glucose and glutamine.
- NPs and MPs exposure acts as a cancer risk factor for human health.

GRAPHICAL ABSTRACT

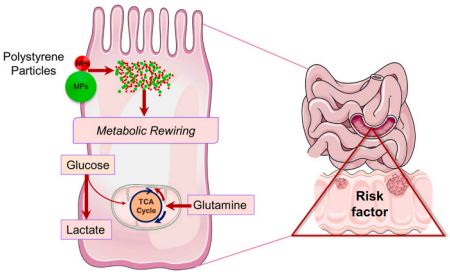

ARTICLE INFO

Handling Editor: Michael Bank

Keywords:
Plastic pollution

ABSTRACT

Polystyrene is a thermoplastic polymer widely used in commercial products. Like all plastics, polystyrene can be degraded into microplastic and nanoplastic particles and ingested via food chain contamination. Although the ecological impact due to plastic contamination is well known, there are no studies indicating a carcinogenic potential of polystyrene microplastics (MPs) and nanoplastics (NPs).

Abbreviations: 1P-3H-5C, 1-Pyrroline-5-carboxylate; 3 PG, 3-Phosphoglycerate; 4-H-Glu, 4-Hydroxyglutamate semialdehyde; 6PGLac, 6-Phosphonoglucono-D-Lactone; AdeSucc, Adenylsuccinic acid; Ado, Adenosine; ADP, Adenosine diphosphate; AKG, α-ketoglutarate; AlloCys, Allocystathionine; AmSug Metab, Amino-Sugar metabolism; AOM, Azoxymethane; Asp, Aspartic acid; CCK-8, Cell Counting Kit-8; Cit, Citric acid; CYT D, Cytochalasin D; DYN, Dynole 34-2; ECAR, Extracellular Acidification Rate; F1,6BP, Fructose 1,6-bisphosphate; F6P, Fructose 6-phosphate; Fum, Fumaric acid; G3P, Glyceraldehyde 3-phosphate; G6P, Glucose 6-phosphate; GDP-Glc, GDP-glucose; GEN, Genistein; Glc, Glucose; Glc-Ala Cycle, Glucose-Alanine Cycle; Gln, Glutamine; Glu 5-P, Glutamic acid 5-phosphate; Glu Metab, Glutamate Metabolism; Glu, Glutamic acid; Glyc 3-P, Glycerol 3-phosphate; Glyc, Glycolysis; GNG, Gluconeogenesis; GSH Metab, Glutathione Metabolism; GSH, Reduced glutathione; GSSG, Oxidized Glutathione; GTP, Guanosine triphosphate; IsoCit, Isocitric acid; Lac, Lactic acid; Mal, Malic acid; Mal-Asp Shuttle, Malate-Aspartate Shuttle; MP(s), Microplastic(s); NH_3 Recyc, Ammonia Recycling; NP(s), Nanoplastic(s); OAA, Oxaloacetic acid; OCR, Oxygen Consumption Rate; OXPHOS, Mitochondrial Oxidative Phosphorylation System; PIT, Pitstop 2–100; PMA, Phorbol 12-myristate 13-acetate; Ppi, Pyrophosphate; Pro, Proline; Pur Metab, Purine metabolism; Pyr, Pyruvic acid; PyrGlu, Pyroglutamic acid; Ribulose 5P, Ribulose 5-phosphate; ROS, Reactive Oxygen Species; Sedo 7P, Sedoheptulose 7-phosphate; Ser, Serine; Succ, Succinic acid; SuccSA, Succinic acid semialdehyde; TCA Cycle, Tricarboxylic acid Cycle; UAC, Uric acid; UDP-Glc, UDP-Glucose; UDP-GlcNAc, Uridine diphosphate-N-acetylglucosamine; γGC, γ-Glutamylcysteine.

* Corresponding author. Institute of Molecular Bioimaging and Physiology (IBFM), National Research Council (CNR), Via Fratelli Cervi 93, 20090, Segrate, MI, Italy.
E-mail address: daniela.gaglio@ibfm.cnr.it (D. Gaglio).

https://doi.org/10.1016/j.chemosphere.2022.134947
Received 14 March 2022; Received in revised form 5 May 2022; Accepted 9 May 2022
Available online 14 May 2022
0045-6535/

Metabolomics
Risk factor

Here, we evaluated the effects of the MPs and NPs on normal human intestinal CCD-18Co cells. Our results show that internalization of NPs and MPs induces metabolic changes under both acute and chronic exposure by inducing oxidative stress, increasing glycolysis via lactate to sustain energy metabolism and glutamine metabolism to sustain anabolic processes. We also show that this decoupling of nutrients mirrors the effect of the potent carcinogenic agent azoxymethane and HCT15 colon cancer cells, carrying out the typical strategy of cancer cells to optimize nutrients utilization and allowing metabolic adaptation to environmental stress conditions. Taken together our data provide new evidence that chronic NPs and MPs exposure could act as cancer risk factor for human health.

1. Introduction

Plastics brought enormous advantages to current habits, playing a central role in our daily life due to their chemical and mechanical properties such as lightweight, resistance, versatility and durability (Andrady and Neal, 2009; Thompson et al., 2009). Although plastic is widely used in several commercial areas (cosmetics, toys, food packaging, domestic use, industrial applications and medical devices) (Groh et al., 2019; Lei et al., 2017; Liu et al., 2019; Marsh and Bugusu, 2007), it is sometimes misused and discarded after a single use (Yee et al., 2021).

Microplastics are mainly divided into primary and secondary microplastics. Primary microplastics are released into the environment by cosmetics, medical products and/or industrial raw materials, while secondary microplastics are mainly derived from decomposition of plastic wastes leading to their gradual breaking down into smaller particles (van Wijnen et al., 2019).

Microplastic (MP) and nanoplastic (NP) particles generated by exposure to environmental factors (such as UV–visible light, oxidation, natural erosion and/or marine corrosion) are becoming an enormous problem for the environment and for human health (Chang et al., 2020; Jiang et al., 2020). MPs and NPs enter the human body by inhalation and/or food and drinks consumption (Yee et al., 2021; Zarus et al., 2021). Several reports show accumulation of MP and NP particles in seafood (Li et al., 2015; Neves et al., 2015a, 2015b; Ribeiro et al., 2020), but fragments are found along the whole food chain (Huerta Lwanga et al., 2017; Toussaint et al., 2019). Distribution of MPs and NPs have been detected in fruit and vegetables (apples and carrots the most contaminated), honey, sugar, salt and beer (Kosuth et al., 2018; Liebezeit and Liebezeit, 2013; Oliveri Conti et al., 2020; Yang et al., 2015).

A recent study conducted on tap, bottled and spring water using Fourier Transform Infrared Spectroscopy (FTIR) showed that MPs are present in all water sources analyzed. Tap water from 159 global sources was tested and 81% of samples contained MP particles smaller than 5 mm (Kosuth et al., 2018). Tests were also conducted on 259 water bottles of 11 different brands and 27 different batches and the results showed that 93% of samples contained MP particles (Mason et al., 2018). High levels of MPs were detected by micro-Raman spectroscopy in mineral water bottled in 22 different multi-use plastics (compared to single-use plastics or cardboard containers), as well as in glass bottles (Schymanski et al., 2018). Other tests conducted on polystyrene cup lids showed that NPs formed over time as the material was degraded (Lambert and Wagner, 2016). Furthermore, Cox and colleagues calculated that an individual consumes 39000-52000 MPs annually with the diet (value calculated on the consumption of sugar, salt, beer, fruit, vegetables, which represent 15% of a normal diet). The value of MPs/NPs would increase if we considered meat, fish, etc. To these calculated amounts, we should add 90000 MPs if consuming only bottled water, compared to 4000 MPs for those who drink only tap water (Cox et al., 2019). The food and drinking water contamination make plausible an estimated microplastic ingestion of about 0.1–5 g average per week via diet (Senathirajah et al., 2021).

Although recent studies indicate that the most significant way humans consume plastic particles is via ingestion (Lehner et al., 2019), few reports examine the toxicity of MPs and NPs on human health, in particular their tumorigenic potential or the effect on metabolism of healthy intestinal cells. To date, MPs are known to accumulate in the human placenta (Ragusa et al., 2021), human blood (Leslie et al., 2022) and in intestines, liver and kidneys of mice treated with polystyrene MPs (Deng et al., 2017). In addition, polystyrene particles have been shown to affect hepatic metabolism, as well as toxicity, oxidative stress and viability of mixed neuronal cultures (Deng et al., 2017). Recent studies show that MPs exposure can cause intestinal disorders, as they can trigger the alteration of the intestinal barrier, which in turn may cause fatty acid and amino acid metabolism disorders. (Fackelmann and Sommer, 2019; Li et al., 2020; Qiao et al., 2019). Moreover, given the deep interconnection of metabolic networks, altered concentrations of metabolites could lead to a deficiency of specific enzymes, transporters and/or altered enzymatic activities affecting linked metabolic pathways (Sullivan et al., 2016; Jans et al., 2022).

Metabolomics-mass spectrometry is a well-established technology for studying metabolic changes or abnormal metabolisms by detection of metabolites related to the physio-pathological state of the cell, tissue or organism. It allows a global assessment of a cellular state within the context of the environmental condition, genetic regulation, altered kinetic activity of enzymes and changes in metabolic reactions. Metabolomics profiling identifying thousands of metabolites generated by the enzymatic reactions of specific metabolic pathways, provide a snapshot of cell activity such as cell signaling, energy transfer, and cell-to-cell communication. Moreover, alternative metabolic routes due to environmental adaptation or acquired drugs resistance may be identified using labeled substrates (stable isotope tracers). For this reason, in recent years, metabolomics finds application in multiple areas, from the discovery of novel mechanisms and new biomarkers to food, nutrition, health and clinics.

In this study, we perform metabolomics analyses to evaluate the effects of polystyrene particles on the CCD-18Co normal human intestinal cell model. Polystyrene is a thermoplastic aromatic polymer that, similar to all plastic, can be degraded into MPs and NPs, and ingested via food chain contamination (Kik et al., 2020). In particular, we used MPs 2 μm in diameter (20 μg/ml) and NPs 0.5 μm in diameter (5 μg/ml). Our results indicate that NPs are internalized early (by 48 h) and easily removed (during a 4 weeks chronic exposure). Instead, MPs accumulate after chronic 4 weeks treatments, but hardly removed. Furthermore, we show that both MPs and NPs are able to induce oxidative stress and a basal metabolic rewiring similar to azoxymethane (AOM) a potent carcinogenic agent, thus contributing to human health risk factors.

2. Materials and methods

2.1. Cell culture

Normal human intestinal CCD-18Co cells were routinely grown in Minimal Essential Medium (MEM) supplemented with 10% Fetal Bovine Serum (FBS), 2 mM glutamine, 1 mM sodium pyruvate and non-essential amino acids (NEAA). HCT15 colon adenocarcinoma cell line and U-937 monocyte cells were grown in Roswell Park Memorial Institute (RPMI) 1640 supplemented with 10% FBS and 2 mM glutamine. All media were supplemented with 100 U/ml penicillin and 100 μg/ml streptomycin. Cells were grown at 37 °C in a 5% CO_2 incubator. Cell lines were obtained from the American Type Culture Collection (ATCC) (LGC

Standard, Teddington, UK). MEM and NEAA were purchased from Sigma-Aldrich (St Louis, MO, USA). All other cell culture reagents were purchased from Life Technologies (Waltham, MA, USA).

2.2. Cells exposure to NPs, MPs and AOM

CCD-18Co cells were plated at a density of 1.5×10^4 cells/cm^2 in 6-well, 12-well or 96-well plates in complete growth medium. After 18 h, cells were exposed to fluorescent carboxylate-modified polystyrene beads with a mean particle size of 0.5 μm (3.6*10^7 particles/ml Nanoplastics, NPs) representative of the nano size or 2 μm (2.32*10^6 particles/ml Microplastics, MPs) representative of the micro size (Fig. 1A) (da Costa et al., 2016; Gigault et al., 2018; Yong et al., 2020) purchased from Sigma-Aldrich. Pub. NO.: US 2004/0139565 A1 July 22, 2004.

To assess the toxic doses of beads, in the absence of a universal method for the conversion of the concentrations between human intake and *in vitro* experiments (Danopoulos et al., 2022), cells were exposed for 48 h to different concentrations (1-5-10-20 μg/ml) of NPs or MPs consistent with published data (Wang et al., 2020; Wu et al., 2019).

For short-term experiments, cells were exposed for 48 h to 5 μg/ml of NPs or 20 μg/ml of MPs, or to 5 and 10 μg/ml of azoxymethane (AOM) (Sigma-Aldrich).

For long-term experiments, cells were continuously exposed for 28 days to 5 μg/ml of NPs, or 20 μg/ml of MPs (washing, splitting and adding new plastics every 7 days), or exposed on alternate weeks (7 days of plastics exposure followed by 7 days without plastics, up to 28 days). For AOM chronic treatment, cells were treated with 5 or 10 μg/ml of AOM for 6 weeks (washing, splitting and renewing the treatment every 7 days).

2.3. NPs and MPs uptake

2.3.1. Flow cytometry analysis

After plastics exposure, cells were washed with PBS and then collected in 500 μl of PBS/5% FBS for analysis. Ten thousand gated events were analyzed by flow cytometry on a CytoFlex S (Beckman Coulter, Brea, CA, USA). PE channel was used to detect cells with internalized plastics. The percentage of stained cells was determined using CytExpert 2.0 software (Beckman Coulter).

2.3.2. Microscopy analysis

Cells were plated in 4-compartments CellView culture slides with glass bottom (GreinerBioOne, Kremsmünster, Austria). After plastics exposure, cells were washed with PBS and fixed with 4% paraformaldehyde for 15 min at room temperature. Cells were then permeabilized with 0.1% Triton X-100 in PBS for 15 min at room temperature. Actin and nuclei were stained with 0.33 μM AlexaFluor488 Phalloidin (Cell Signaling Technology, Danvers, MA, USA) and 10 μg/ml Hoechst-3342 (Life Technologies), respectively, for 30 min at room temperature. Cells were washed with PBS and images were acquired using an A1R confocal microscope (Nikon, Tokyo, Japan) with 40 × magnification.

2.4. Cell proliferation and cytotoxicity analyses

Cells were collected after 48 h of plastics treatment and counted using a Countess® II FL Automated Cell Counter (Thermo Fisher Scientific, Waltham, MA, USA). A Cell Counting Kit-8 (CCK-8) assay (Sigma-Aldrich) was used to measure the cytotoxicity of NPs and MPs. The assay is based on the conversion of a water-soluble tetrazolium salt (WST-8) to a water-soluble formazan dye upon reduction by dehydrogenases in the presence of an electron carrier. Briefly, CCD-18Co cells were plated in a 96-well plate and after 48 h of plastics exposure, 10 μl of CCK-8 were added to each well, followed by incubation for 2 h at 37 °C. Absorbance was read at 450 nm in a Victor 3 microplate reader (PerkinElmer, Shelton, CT, USA). Cell viability was expressed as a percentage of control cells.

2.5. ROS levels measurement

ROS levels were measured using the DCFDA Cellular ROS Detection Assay Kit (Abcam, Cambridge, UK). Cells were stained with 20 μM dichloro-dihydro-fluoresceine-diacetate (DCFDA) for 30 min at 37 °C. Thereafter, cells were washed and collected in 500 μl of PBS/5%FBS for analysis. Ten thousand gated events were analyzed by flow cytometry on a CytoFlex S (Beckman Coulter, Brea, CA, USA), using FITC channel. The median fluorescence intensity of cells were determined using CytExpert 2.0 software (Beckman Coulter).

2.6. NPs and MPs uptake mechanism

To characterize mechanisms of plastics uptake, CCD-18Co were treated with the indicated inhibitors of endocytosis prior to exposure to NPs and MPs. Briefly, cells were pre-treated with different endocytosis inhibitors for 1 h at 37 °C at the following concentrations: 20 μM Cytochalasin D (Cayman Chemical, Ann Harbor, MI, USA), 40 μM Genistein (Sigma-Aldrich), 20 μM Pitstop 2–100 (Abcam), 5 μM Dynole 34-2 (Abcam). Then, inhibitors were removed and cells were exposed to 5 μg/ml NPs or 20 μg/ml MPs for 4 h at 37 °C. To assess passive internalization of plastics, experiments were also conducted at 4 °C for 4 h. Plastics internalization was detected using flow cytometry. Ten thousand gated events were analyzed by a CytoFlex S (Beckman Coulter), using PE channel. The median fluorescence intensity of cells was determined using CytExpert 2.0 software (Beckman Coulter). Data were expressed as normalized to control cells.

2.7. Seahorse analyses

Cellular oxygen consumption rate (OCR) and extracellular acidification rate (ECAR) were measured by Seahorse XF extracellular flux analyzer (Seahorse Bioscience Inc., North Billerica, MA, USA) according to the manufacturer's instructions. Briefly, cells were seeded in Seahorse XF 24-well assay plates at a cell density of 30000 cells per well in normal growth medium. After overnight attachment, medium was washed and replaced with pre-warmed assay medium (non-buffered DMEM supplemented with 1 mM sodium pyruvate, 5.5 mM glucose and 2 mM glutamine, pH 7.4 for mitochondrial stress test, or non-buffered DMEM supplemented with 2 mM glutamine, pH 7.4 for glycolysis stress test), and incubated in a non-CO_2 incubator at 37 °C for 1 h.

For mitochondrial stress test, OCR was recorded at basal level and after injection of ATP synthase inhibitor oligomycin (1 μM), the uncoupler FCCP (1 μM), or the electron transport inhibitor rotenone/antimycin A (0.5 μM). The following formulas were used to calculate respiratory parameters: Basal Respiration = $OCR_{basal} - OCR_{rot/ant}$. Maximal Respiration = $OCR_{FCCP} - OCR_{rot/ant}$. Spare respiratory capacity = Maximal respiration – Basal Respiration. ATP production: $OCR_{basal} - OCR_{oligo}$.

For glycolysis stress test, ECAR was recorded at basal level and after injection of glucose (10 mM), the ATP synthase inhibitor oligomycin (1 μM) or the glycolysis inhibitor 2-Deoxy-D-glucose (2-DG) (50 mM). The following formulas were used to calculate glycolysis parameters: Glycolysis = $ECAR_{glc} - ECAR_{2\text{-}DG}$. Glycolytic Capacity = $ECAR_{oligo} - ECAR_{2\text{-}DG}$. Glycolytic Reserve = $ECAR_{oligo} - ECAR_{glc}$.

2.8. Metabolites extraction

CCD-18Co were plated in 6-well plates with normal growth medium as described in section 2.2. HCT15 were plated in 6-well plates at a density of 1×10^4 cells/cm^2. For untargeted experiments, after 18 h cells were washed with PBS and incubated for 48 h in fresh complete medium in the presence or the absence of plastics. For labelling experiments, cells

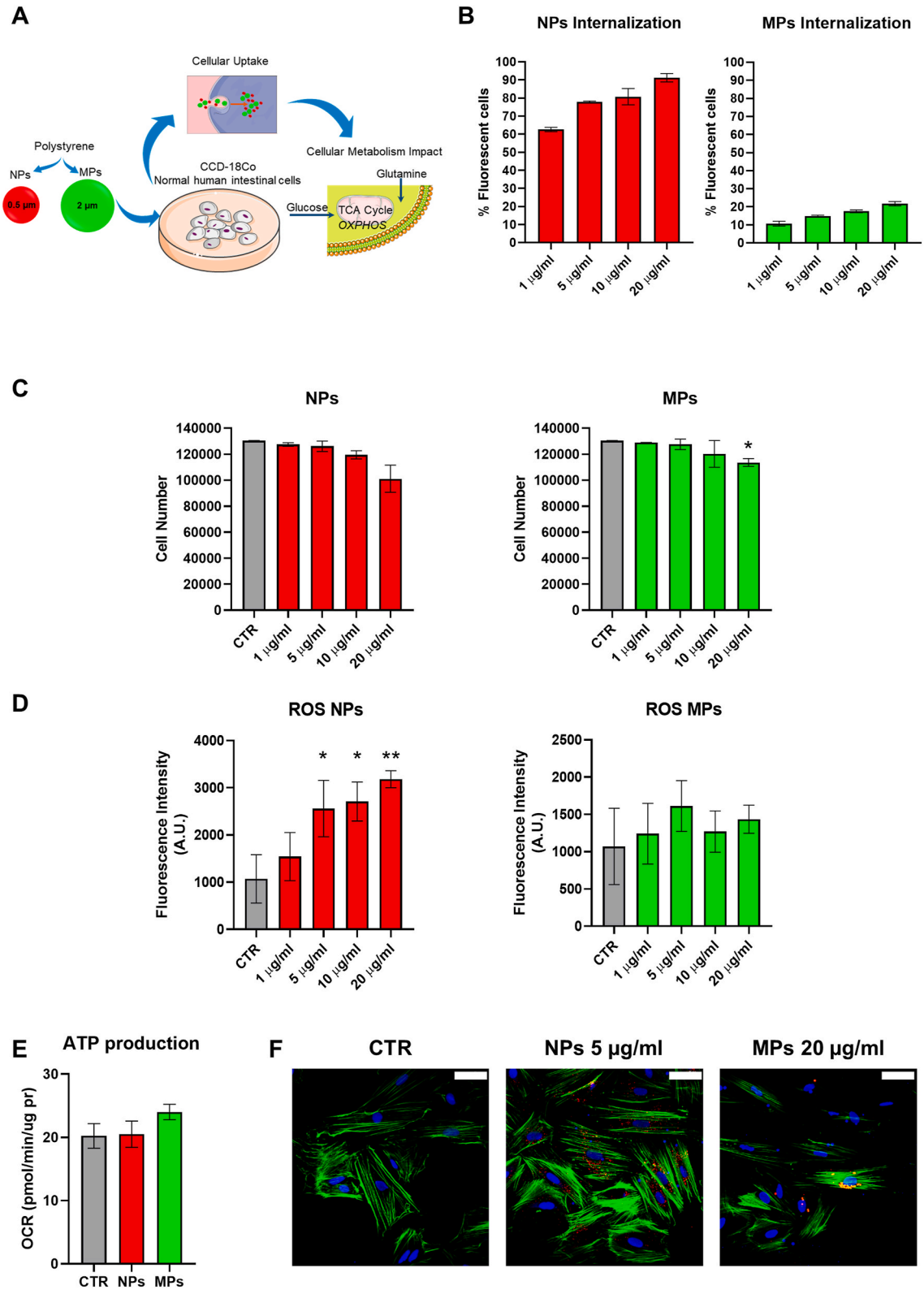

Fig. 1. Internalization of micro- and nano polystyrene particles in normal human intestinal CCD-18Co cells. A) Schematic representation of experimental design (polystyrene particles: 0.5 μm NPs, red color and 2 μm MP, green color). B) Internalization of particles in CCD-18Co cells exposed to fluorescent NPs and MPs at concentrations of 1-5-10 and 20 μg/ml for 48 h measured by flow cytometry analysis. Data are expressed as percentage of fluorescent cells (n = 3). C) Cell viability of CCD-18Co cells after 48 h of exposure to 1-5-10 and 20 μg/ml of NPs and MPs. Data are expressed as mean cell number (n = 3). D) Intracellular ROS levels measured by DCFDA staining after 48 h exposure to NPs and MPs by flow cytometry analysis. Data are expressed as mean fluorescence intensity (n = 3). E) Mitochondrial ATP reflected by OCR levels assessed by Mitostress Seahorse analysis after 48 h exposure to NPs and MPs (n = 5). F) Confocal images of CCD-18Co cells control (CTR, left) and exposed for 48 h to fluorescent NPs (middle), and MPs (right) polystyrene particles. Green: actin filaments; blue: nuclei; red: polystyrene particles. Scale bars = 50 μm. Error bars indicate SD. *$p \leq 0.05$, **$p \leq 0.01$. (For interpretation of the references to color in this figure legend, the reader is referred to the Web version of this article.)

were incubated for 48 h in fresh media supplemented with 25 mM [U-$^{13}C_6$]glucose or 2 mM [U-$^{13}C_5$]glutamine (purchased by Cambridge Isotope Laboratories, Tewksbury, MA, USA).

Metabolites extraction for GC-MS analysis was performed as described previously (Gaglio et al., 2016). Briefly, cells were quenched with 1:1 ice-cold methanol:water and collected by scraping. After sonication, one volume of chloroform was added, and cells were vortexed at 4 °C for 20 min. Samples were centrifuged at 12000 g for 10 min, and the aqueous phase was collected in a glass insert and dried in a centrifugal vacuum concentrator (Concentrator plus/Vacufuge plus, Eppendorf, Hamburg, Germany) at 30 °C for about 2.5 h.

For metabolites extraction for LC-MS analysis, cells were quickly rinsed with NaCl 0.9% and quenched with 500 μl ice-cold 70:30 acetonitrile:water. Plates were placed at −80 °C for 10 min, then cells were collected by scraping and sonicated 5 s for 5 pulses at 70% power twice. Samples were centrifuged at 12000g for 10 min and supernatants were collected in a glass insert and dried in a centrifugal vacuum concentrator (Concentrator plus/Vacufuge plus, Eppendorf) at 30 °C for about 2.5 h. Samples were then resuspended with 150 μl H_2O prior to analyses.

2.9. GC-MS metabolic profiling

Dried polar metabolites were dissolved in 60 μl of 2% methoxyamine hydrochloride in pyridine (Thermo Fisher Scientific) and held at 40 °C for 6 h. After the reaction, 90 μl of MTBSTFA +1% TBDMCS (Thermo Fisher Scientific) were added and samples were incubated at 60 °C for 1 h. Derivatized samples were analyzed by GC-MS using a DB-35MS column (30 m × 0.25 mm x 0.25 μm) installed in an Agilent Intuvo 9000 gas chromatograph (GC) interfaced with a 5977B mass spectrometer (MS) (Agilent Technologies, Santa Clara, CA, USA) operating under electron impact (EI) ionization at 70 eV. Samples (2 μl) were injected in splitless mode at 270 °C, using helium as the carrier gas at a flow rate of 1 ml/min. The GC oven temperature was held at 100 °C for 3 min and increased to 300 °C at 3.5 °C/min. Data were pre-processed using the OpenChrom software package to convert raw data (.D) in NetCDF format. Mass isotopologue distributions (MIDs) were determined using Matlab by integrating metabolite ion fragments and correcting for natural abundance using in-house algorithms adapted from (Antoniewicz, 2018).

2.10. LC-MS metabolic profiling

LC separation was performed using an Agilent 1290 Infinity UHPLC system and an InfintyLab Poroshell 120 PFP column (2.1 × 100 mm, 2.7 μm; Agilent Technologies). Mobile phase A was water with 0.1% formic acid. Mobile phase B was acetonitrile with 0.1% formic acid. The injection volume was 15 μL and LC gradient conditions were: 0 min: 100% A; 2 min: 100% A; 4 min: 99% A; 10 min: 98% A; 11 min: 70% A; 15 min: 70% A; 16 min: 100% A with 5 min of post-run. Flow rate was 0.2 ml/min and column temperature was 35 °C. MS detection was performed using an Agilent 6550 iFunnel Q-TOF mass spectrometer with Dual JetStream source operating in negative ionization mode. MS parameters were: gas temp: 285 °C; gas flow: 14 l/min; nebulizer pressure: 45 psig; sheath gas temp: 330 °C; sheath gas flow: 12 l/min; VCap: 3700 V; Fragmentor: 175 V; Skimmer: 65 V; Octopole RF: 750 V. Active reference mass correction was done through a second nebulizer using masses with *m/z*: 112.9855 and 1033.9881. Data were acquired from *m/z* 60–1050. Data analysis and isotopic natural abundance correction were performed with MassHunter ProFinder and MassHunter VistaFlux software (Agilent) (Bonanomi et al., 2021).

2.11. Circos plots analysis

CIRCOS plots (Krzywinski et al., 2009) were constructed using table viewer (http://mkweb.bcgsc.ca/tableviewer/). Common metabolites and pathways identified using Metaboanalyst 5.0 are shown outside of the circle.

2.12. Monocytes differentiation assay

U-937 cells (1 × 10^5/well) were cultured in 6-well plates in 1 ml of medium in the presence or the absence of 5 μg/ml of NPs or 20 μg/ml of MPs for 120 h. After washing with PBS, adherent cells on the wells were imaged under a DMi1 light microscope equipped with a MC170HD camera (Leica, Wetzlar, Germany) with 10X magnification. To induce monocyte differentiation as positive control, cells were stimulated with 10 ng/ml of phorbol 12-myristate 13-acetate (PMA, Sigma-Aldrich) for 120 h.

2.13. Quantification and statistical analysis

All experiments were performed at least in triplicate. Data are presented as mean ± SD. Observed differences were tested for significance with Student's t-test. For metabolomics experiments, statistical and enrichment analyses were performed by Mass Profiler Professional (MPP) and Metaboanalyst 5.0 software. Statistics are included in figure legends.

3. Results

Polystyrene is an extensively used polymer (Kik et al., 2020); the effects of ingestion of its degradation products into MPs and NPs on metabolism of human colon cells are not yet known. Here we employed *in vitro* CCD-18Co normal human intestinal cell model to assess the impact on metabolism of polystyrene NPs and MPs, with a diameter of 0.5 μm and 2 μm respectively (Fig. 1A) (Yong et al., 2020). To investigate the internalization of NPs and MPs, we exposed normal human CCD-18Co cells to different concentrations (Lim et al., 2019; Wang et al., 2020; Wu et al., 2019) of fluorescent particles for 48 h, and measured NPs and MPs fluorescence by flow cytometry (Fig. 1B). We found a significantly higher percentage of cells with NPs internalization (70%–90%) as compared to MPs (10%–20%), that suggests an easier internalization of NPs in CCD-18Co cells after 48 h exposure (Fig. 1B). To elucidate biochemical events underlying the dynamic process of particles internalization, we performed treatments with: i) Cytochalasin D (CYT D), an inhibitor of phagocytosis and macropinocytosis blocking actin polymerization and inducing disassembly of the actin cytoskeleton; ii) Pitstop 2–100 (PIT), a clathrin N-terminal domain inhibitor; iii) Dynole 34-2 (DYN), a dynamin I and dynamin II inhibitor (dynamin dependent); iv) Genistein (GEN), a caveolae-mediated uptake inhibitor; or incubation at 4 °C for 4 h to evaluate energy-independent penetration (passive transport) (Liu et al., 2021) (Figure S1A). The amount of internalized particles decreases under CYT D inhibitor treatment, indicating a similar clathrin-mediated endocytosis uptake mechanism for both NPs and MPs, as further confirmed for MPs by PIT inhibition (Figure S1A). Moreover, the decreased internalization of NPs under 4 °C condition suggests that NPs uptake occurs exclusively through an energy dependent internalization process, as compared to MPs, which even show an additional passive transport mechanism (Figure S1A).

Despite the involvement of different internalization modes, we observed that none of particles concentrations causes cell mortality or cytotoxicity (Figure S1B) (Deng et al., 2017), decreased cell proliferation is found exclusively with the dose of 20 μg/ml for MPs (Fig. 1C). On the other hand, we found significantly increased ROS levels after 48 h of 5–10 and 20 μg/ml of NPs exposure, as compared to control and MPs treatments (Fig. 1D). Since mitochondria are the main source of ROS and energy, we examined mitochondrial function (Figure S1C). Seahorse analysis, however, does not show significant differences in terms of ATP production and mitochondrial activity (Fig. 1E), but a significant decrease in maximal respiration and spare respiratory capacity (Figure S1C), suggesting that polystyrene particles partially interfere

with mitochondrial complexes activity in CCD-18Co after 48 h of NPs and MPs exposure. These observations of cellular uptake and basal metabolic characterization prompted us to perform further detailed metabolic analysis with selected particles concentration: 5 μg/ml for NPs and 20 μg/ml for MPs (Fig. 1F).

3.1. Short exposure to polystyrene NPs induces early metabolic rewiring in normal human colon cells

To better study the metabolic impact of polystyrene NPs and MPs on normal human colon CCD-18Co cells, we performed detailed metabolomics mass spectrometry analysis. Azoxymethane (AOM), a potent carcinogenic agent commonly used to induce colon cancer in rats (Al-Numair et al., 2012; Waly et al., 2012), was used to investigate the potential carcinogenic impact of polystyrene MPs and NPs exposure.

Hierarchical clustering of metabolic profiling shows similar metabolic signatures between NPs and 10 μg/ml AOM after 48 h, as compared to control, MPs and 5 μg/ml AOM (Fig. 2A). Pathway enrichment analysis of all significant metabolites data set suggests the involvement of Warburg effect, as well as amino acids and redox metabolism alterations (Fig. 2A). Specifically, 47 significant metabolites are common between NPs exposure and AOM treatment (Fig. 2B). Moreover, cross-analysis of these common significant metabolites and cognate enriched pathways provides the first indication that pathways, such as: Warburg effect, glutamate metabolism and glutathione metabolism are involved in early metabolic rewiring under NPs exposure and AOM treatment (Fig. 2B lower panel).

Consistent with these data, we found significantly increased levels of metabolites involved in glycolysis and in glycolytic reserve (Fig. 2C and S1D), TCA cycle and pentose phosphate pathway (PPP) in CCD-18Co cells under NPs, MPs and AOM treatments as compared to control (Fig. 2C). Significantly decreased levels of GSH/GSSG ratio further confirm the redox stress due to NPs and AOM treatments (Fig. 2D). Similar nucleotides and amino acids signatures identify increased glutamine metabolism by NPs, MPs and AOM treatments as compared to control (Fig. 2E).

To confirm that short exposure to NPs induces early metabolic rewiring in human colon cells similar to the carcinogenic AOM, we performed a more in-depth metabolic analysis using [U-$^{13}C_6$]glucose and [U-$^{13}C_5$]glutamine isotope tracers (Fig. 3). The relative increased m+3 lactate incorporation of uniformly labeled [U-$^{13}C_6$]glucose confirms a higher glucose oxidation via lactate in all treatment conditions (Fig. 3A). Moreover, we find increased levels of m+6 6-phosphogluconolactone (6PGLac) coming from glucose and m+5 glutathione (GSH) and proline (Pro) coming from glutamine, both involved in ROS scavengers metabolic pathways, in NPs-treated cells as compared to control and MPs (Fig. 3A and B), which indicate the physiological response to redox stress, as previously observed (Figs. 1 and 2). As expected we find increased canonical labeling of m+2 TCA cycle intermediates coming from glucose as well as increased labeling in m+3 of malate (Mal) and aspartate (Asp) derived from pyruvate carboxylase activity (Fig. 3A). In addition, we also observed increased levels of m+4 TCA cycle metabolites coming from glutamine under short exposure (Fig. 3B). The latter result highlights that cells attempt to adapt their metabolism to metabolic stress conditions, using no longer canonical and physiological ways, but starting to rearrange their metabolism induced by environmental conditions similar to a tumorigenesis process.

3.2. Continuous exposure to polystyrene MPs increases internalization and metabolic rewiring in normal human colon cells

Given that polystyrene particles may be found in commonly used products, we tested the impact of polystyrene particles on long-term exposure. To this end, we investigated the effect of continuous exposure to 5 μg/ml NPs and 20 μg/ml MPs on human normal intestinal CCD-18Co cells for 4 weeks (Fig. 4A, red line). In addition to this chronic exposure of NPs and MPs, we performed intermittent exposures on alternate weeks, in order to assess whether both polystyrene particles might be released and/or induce a metabolic stress recovery (Fig. 4A, blue line).

Flow cytometric measurements of intracellular fluorescence intensity revealed that chronic exposure leads to a significant accumulation of MPs (about 90% of fluorescent cells), suggesting a gradual internalization of MPs with a lower release/recovery, as compared to NPs (Fig. 4B and C). ROS levels are also significantly increased after chronic exposure to both MPs and NPs, and partially restored in the recovery samples (Fig. 4D). However, the recovery function is not observed in terms of metabolism: a significant decrease in mitochondrial function and ATP production is found following NPs and MPs treatments, during both chronic and intermittent exposure; instead, not significant changes can be observed for basal glycolysis under chronic NPs exposure (Fig. 4E and S2A-B). In fact, only a slight change in glycolytic capacity can be appreciated under NPs exposure, as compared to the significant increase in glycolytic flux under chronic MPs exposure (Fig. 4E and S2A-B and C).

To better investigate metabolic changes and the potential carcinogenic impact on metabolism of polystyrene particles, we compared the effect of MPs and NPs (both chronic and recovery treatments) to AOM (chronic, 5–10 μg/ml) on human normal intestinal CCD-18Co cells and the metabolic profile of HCT15 colon rectal cancer cell line as a metabolic advanced cancer model (Fig. 5).

In contrast to acute exposure, hierarchical clustering shows similar metabolic signatures between MPs and AOM after 4 weeks, and HCT15 colon cancer cells in the first main branch (Fig. 5A). Unexpectedly, clustering analysis identifies a sub-cluster including chronic NPs and intermittent MPs exposure, suggesting the lack of metabolic rescue in recovery MPs samples (Fig. 5A).

Similar to acute exposure, pathway enrichment analysis of all significant metabolites data set highlights the involvement of Warburg effect and glutamate metabolism (Fig. 5A, lower panel). Deeper analysis of common metabolites in the first main cluster branch identifies 28 common metabolites between chronic MPs and AOM exposure and 16 common metabolites between the three experimental conditions (Fig. 5B). Specifically, cross-analysis between the 28 most common significant metabolites and cognate enriched pathways provide indication that the metabolic rearrangement observed in MPs and AOM treatments involves key metabolic tumorigenic pathways such as glycolysis, glutathione-glutamate and nucleotides metabolism (Fig. 5B lower panel). Consistent with this indication, we find significantly increased levels of metabolites involved in glycolysis, TCA cycle and pentose phosphate pathways (PPP) (but not in GSH/GSSG ratio) in CCD-18Co cells under MPs and AOM treatments as compared to control, similar to those observed in HCT15 cells (Fig. 5C and D). We even find in the recovery samples increased levels of metabolites involved in the first branch of TCA cycle and GSH/GSSG ratio, suggesting an attempt to re-establish canonical physiological ways (Figure S2C and D). In addition, nucleotides and amino acids metabolism signature identifies once again increased glutamine metabolism under MPs and AOM treatments, as compared to control in normal human CCD-18Co cells as above suggested (Fig. 5E).

The recovery function is not observed in terms of metabolism: a significant decrease in mitochondrial function and ATP production is found following NPs and MPs treatments, during both chronic and intermittent exposure (Figure S2A and B).

3.3. [U-$^{13}C_6$]glucose and [U-$^{13}C_5$]glutamine labeling confirm that long exposure to MPs induces metabolic rewiring in human colon cells

To definitely confirm that long-term exposure of polystyrene particles induces metabolic rewiring in human colon cells similar to the carcinogenic AOM and to HCT15 colon cancer cells, we performed targeted metabolic analysis using [U-$^{13}C_6$]glucose and [U-$^{13}C_5$]glutamine

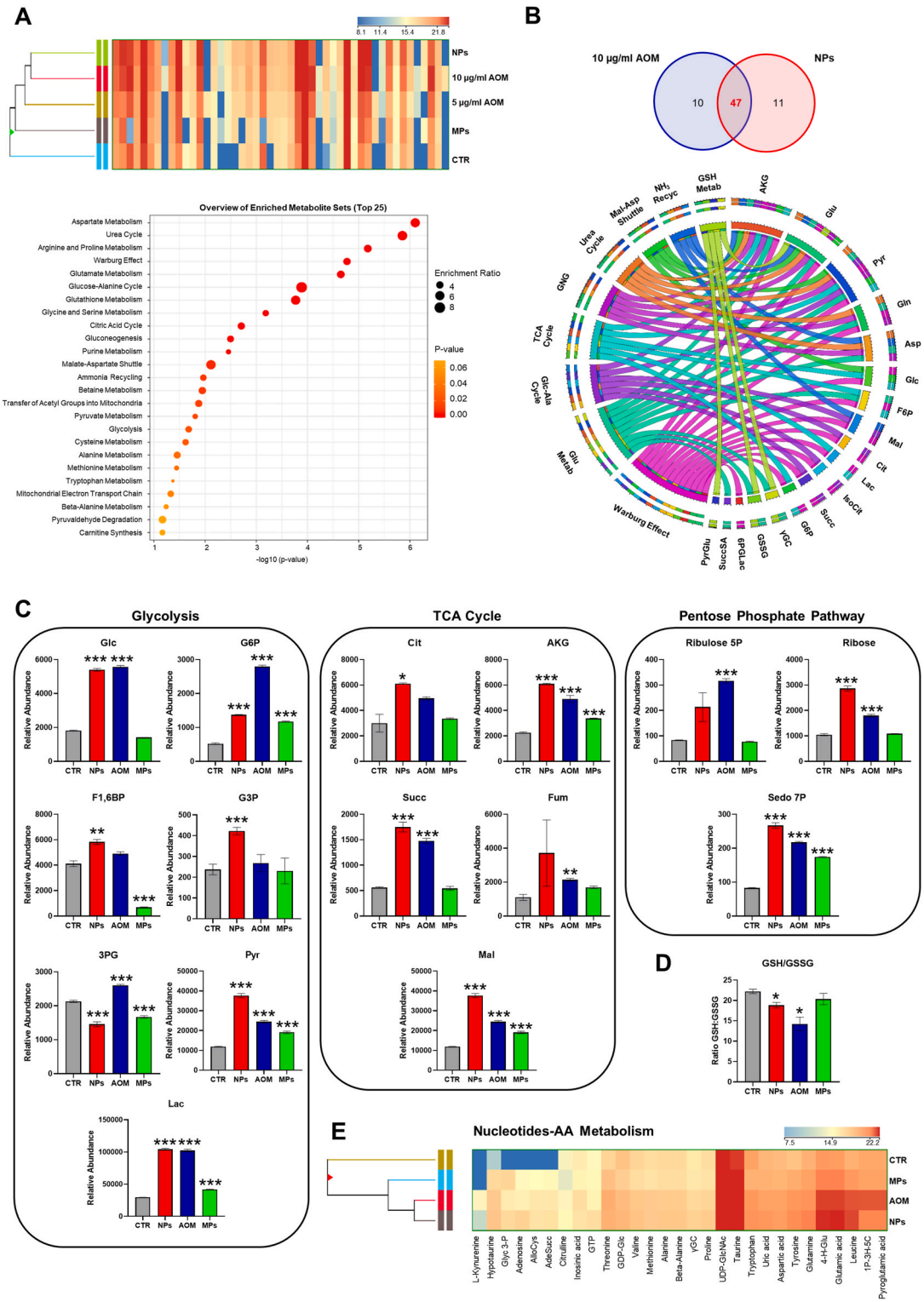

Fig. 2. Untargeted metabolic profiling of normal human intestinal CCD-18Co cells after NPs and MPs exposure. A) Hierarchical clustering heatmap showing significantly different intracellular metabolites by LC-MS (upper panel). Colors represent different levels that increase from blue to red. Quantitative pathway enrichment of differential metabolites obtained by Metaboanalyst 5.0 (lower panel). B) Venn diagram of common significant metabolites between AOM and NPs obtained by MPP (upper panel) and Circos plot (lower panel) showing the most significant metabolites and cognate enriched pathways under AOM treatment and NPs exposure. C) Relative metabolites abundance of glycolysis (left panel), TCA cycle (middle panel) and PPP (right panel) pathways in control CCD-18Co cells or after 48 h of exposure to NPs, MPs or AOM (n = 3). D) GSH/GSSG ratio in CCD-18Co cells after 48 h of exposure to NPs and MPs based on relative abundance obtained by LC-MS analysis. (n = 3). E) Hierarchical clustering heatmap showing significantly different intracellular metabolites involved in nucleotides and amino acids metabolism as detected by LC-MS. Colors represent different levels that increase from blue to red. Error bars indicate SD. *p ≤ 0.005, **p ≤ 0.001. ***p ≤ 0.0005. (For interpretation of the references to color in this figure legend, the reader is referred to the Web version of this article.)

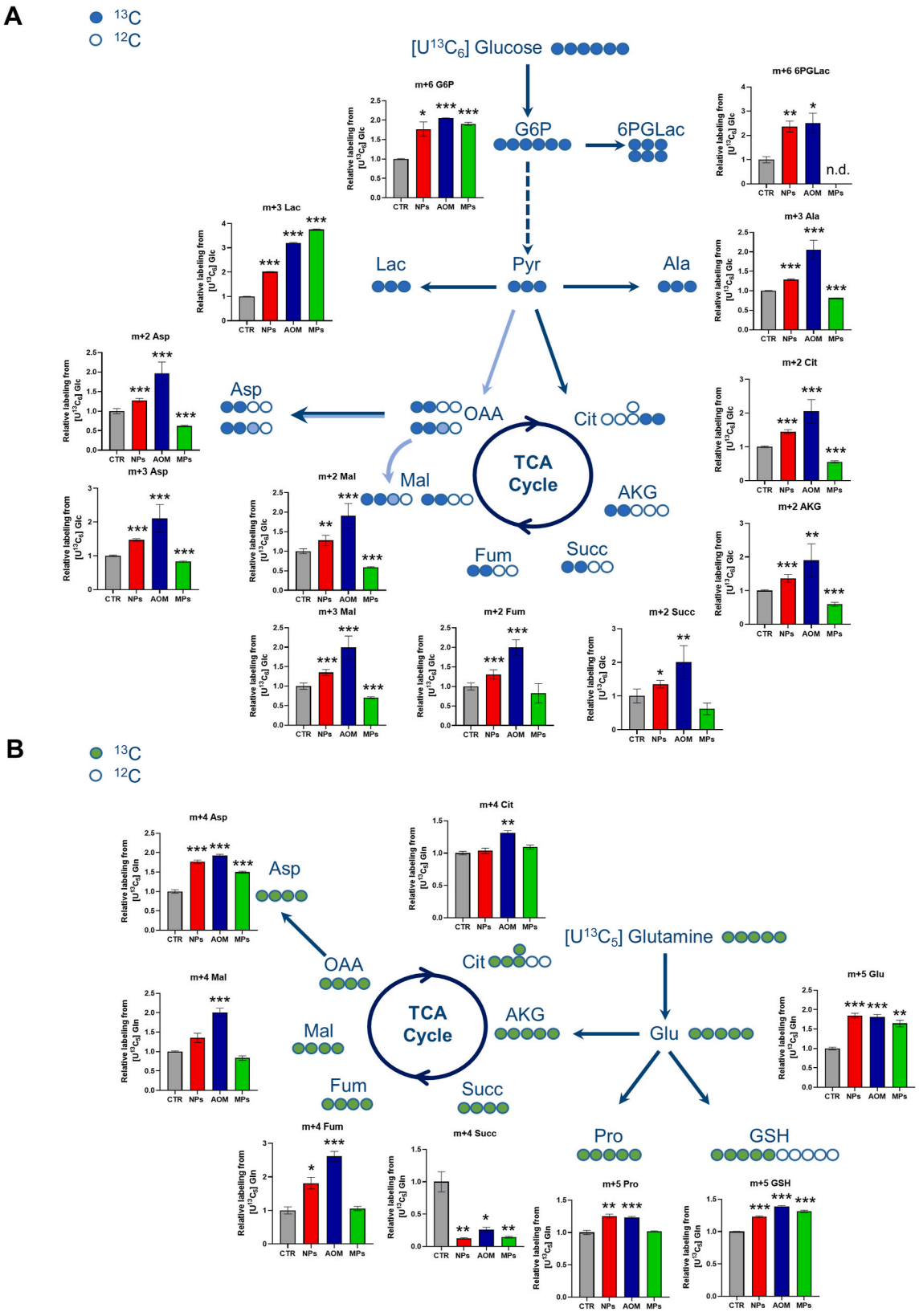

Fig. 3. Early metabolic rewiring in CCD-18Co cells after short NPs exposure by [U-$^{13}C_6$]glucose and [U-$^{13}C_5$]glutamine labeling. A and B) Schematic representations and percentage isotope labeling enrichment of metabolites from [U-$^{13}C_6$]glucose (blue circles) and [U-$^{13}C_5$]glutamine labeling (green circles). Relative labeling obtained by GC-MS and LC-MS analysis. Filled circles indicate ^{13}C enrichment (n = 3). Error bars indicate SD. *p ≤ 0.005, **p ≤ 0.001. ***p ≤ 0.0005. (For interpretation of the references to color in this figure legend, the reader is referred to the Web version of this article.)

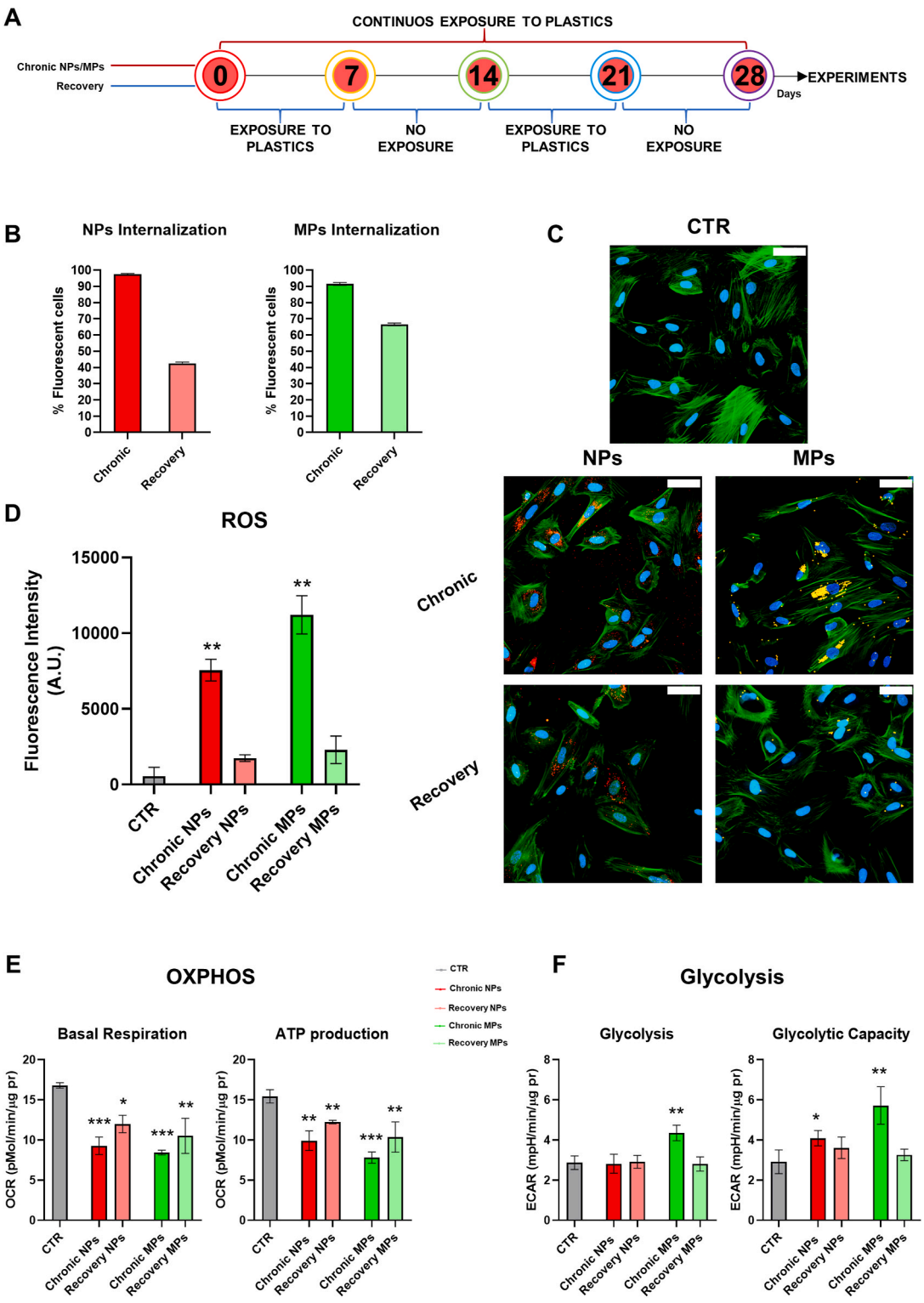

Fig. 4. Chronic exposure of normal human colon CCD-18Co cells to polystyrene NPs and MPs. A) Schematic representation of continuous (red line) and intermittent (blue line) exposure to 5 μg/ml NPs and 20 μg/ml MPs in CCD-18Co cells for 4 weeks. B) Internalization of particles in CCD-18Co cells after chronic or intermittent (recovery) exposure for 4 weeks to 5 μg/ml NPs and 20 μg/ml MPs measured by flow cytometry analysis. Data are expressed as percentage of fluorescent cells (n = 3). C) Confocal images of control CCD-18Co cells (CTR, upper panel) and after chronic or intermittent (recovery) exposure for 4 weeks to 5 μg/ml NPs (left panel) and 20 μg/ml MPs (right panel). Green: actin filaments; blue: nuclei; red: polystyrene particles Scale bars = 50 μm. D) Intracellular ROS levels measured by DCFDA staining in CCD-18Co after continuous and intermittent NPs and MPs exposure. E) Mitochondrial basal respiration and ATP production reflected by OCR levels assessed by Mitostress Seahorse analysis and F) Glycolysis rate and glycolytic capacity reflected by ECAR levels assessed by Glycolysis stress Seahorse analysis measured in CCD-18Co cells after continuous and intermittent NPs and MPs exposure (n = 5). Error bars indicate SD. *p ≤ 0.05, **p ≤ 0.01, ***p ≤ 0.005. (For interpretation of the references to color in this figure legend, the reader is referred to the Web version of this article.)

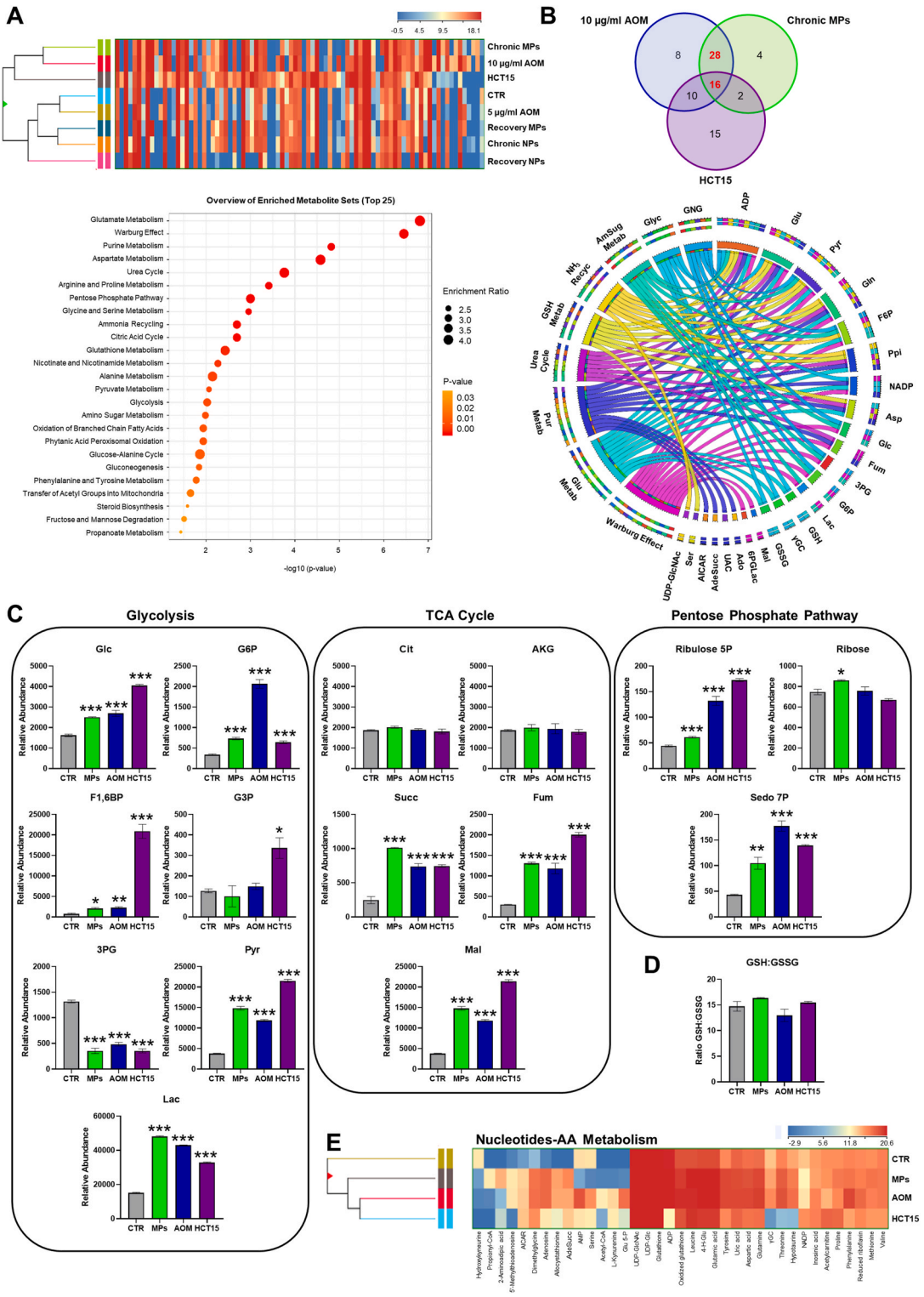

Fig. 5. Metabolic characterization of normal human colon CCD-18Co cells after continuous polystyrene NPs and MPs exposure. A) Hierarchical clustering heatmap showing significantly different intracellular metabolites by LC-MS (upper panel). Colors represent different levels that increase from blue to red. Quantitative pathway enrichment of differential metabolites obtained by Metaboanalyst 5.0 (lower panel). B) Venn diagram of common significant metabolites between AOM, chronic MPs and HCT15 colon cancer cells by MPP (upper panel). Circos plot show the most significant metabolites and cognate enriched pathways under AOM treatment and MPs exposure. C) Relative metabolites abundance of glycolysis (left panel), TCA cycle (middle panel) and PPP (right panel) pathways in control CCD-18Co cells or after chronic exposure to MPs and AOM, and in HCT15 cancer cells (n = 3). D) GSH/GSSG ratio in control CCD-18Co cells or after chronic exposure to MPs and AOM, and in HCT15 cancer cells based on relative abundance obtained by LC-MS analysis (n = 3). E) Hierarchical clustering heatmap showing significantly different intracellular metabolites involved in nucleotides and amino acids metabolism by LC-MS. Colors represent different levels that increase from blue to red. Error bars indicate SD. *p ≤ 0.005, **p ≤ 0.001. ***p ≤ 0.0005. (For interpretation of the references to color in this figure legend, the reader is referred to the Web version of this article.)

isotope tracers (Fig. 6). The relative higher m+3 lactate labeling confirms the increase in glycolysis via lactate in all treatment conditions (Fig. 6A). Although we find significant increased levels of labeling in m+2 TCA cycle intermediates coming from glucose in HCT15 as compared to control CCD-18Co cells, we observe an opposite trend in the same metabolites under chronic MPs and AOM exposure as well as in m+3 of Mal and fumarate (Fum) (Fig. 6A).

On the other hand, the same TCA cycle intermediates are strongly

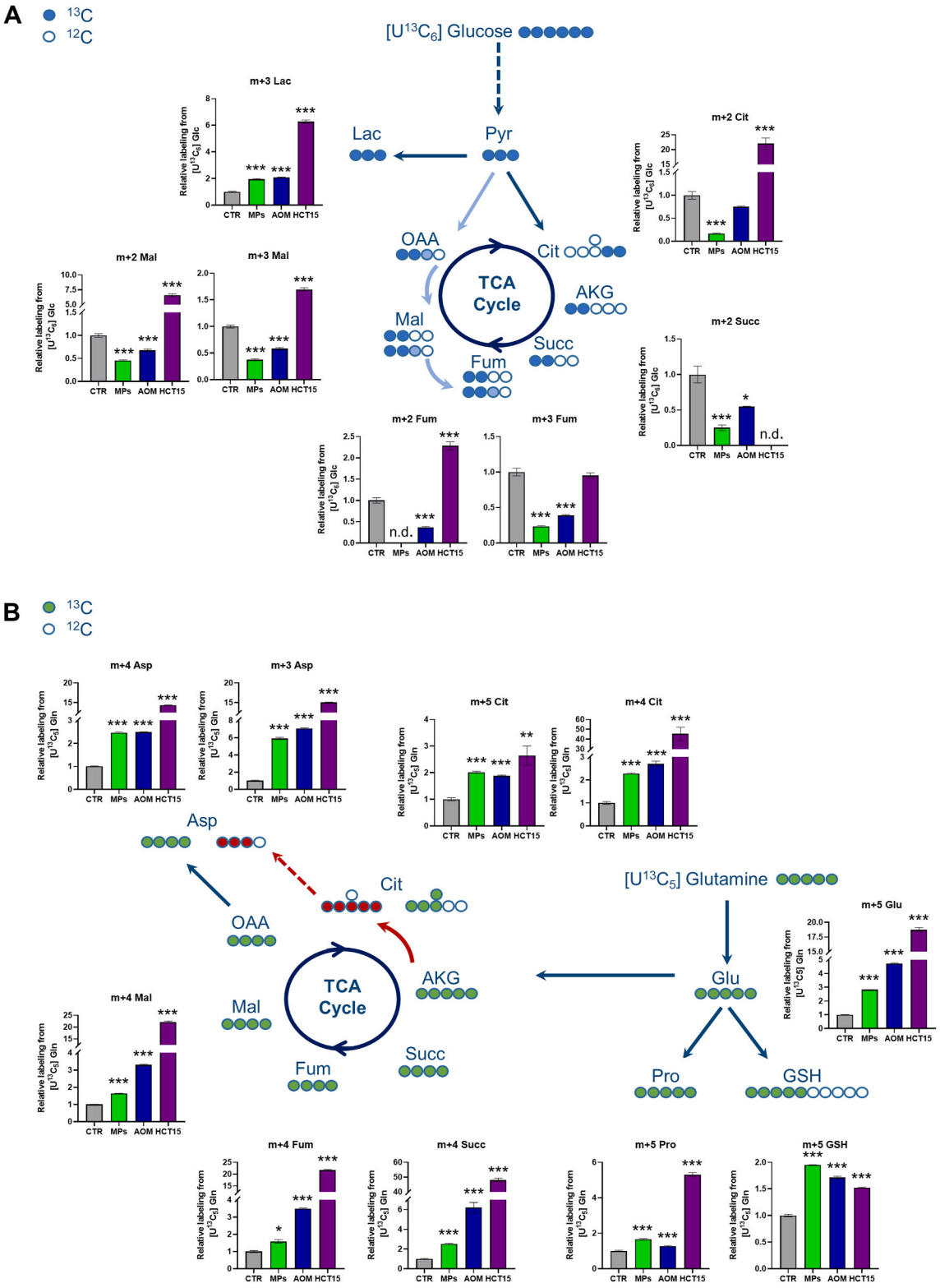

Fig. 6. Metabolic rewiring in CCD-18Co cells after chronic MPs and AOM exposure and in HCT15 colon cancer cells by [U-$^{13}C_6$]glucose and [U-$^{13}C_5$]glutamine labeling. A and B) Schematic representations and percentage isotope labeling enrichment of metabolites from [U-$^{13}C_6$]glucose (blue circles) and [U-$^{13}C_5$]glutamine labeling (green circles). Relative labeling obtained by LC-MS analysis. Filled circles indicate ^{13}C enrichment (n = 3). Error bars indicate SD. *p ≤ 0.005, **p ≤ 0.001. ***p ≤ 0.0005. (For interpretation of the references to color in this figure legend, the reader is referred to the Web version of this article.)

labeled in m+4 using [U-$^{13}C_5$]glutamine tracer (Fig. 6B). Surprisingly, we find labeling coming not only from glutamine in forward TCA cycle intermediates, but even in the reverse cycle (Fig. 6B, red arrow). In fact, labeling of m+5 citrate (Cit) and m+3 Asp can derive only from non-canonical labeled TCA cycle intermediates through reductive carboxylation of glutamine (Fig. 6B). Moreover, we find m+5 GSH and Pro coming from glutamine and involved in ROS scavengers metabolic pathways in all three conditions as compared to control (Fig. 6B). Taken together, these data highlight a perfect decoupling of glucose and glutamine fate. In addition, this initial metabolic plasticity showed by normal human colon cells under polystyrene treatments optimizes nutrients utilization and allows metabolic adaptation to environmental stress condition typical of cancer cells. We also observe that MPs and NPs are internalized (Figure S3A) inducing reduction of proliferation in U-937 monocytes cell line after 48 h exposure (Figure S3B), although they do not induce monocyte differentiation as compared to PMA treatment (Figure S3C). These results could be due to the use of spherical NP and MP particles that might underestimate their immunogenic properties (Weber et al., 2022), so they might not be harmful on our immune cells model.

4. Discussion

Micro- and nanoplastic particles generated by exposure to environmental factors may enter in human body by inhalation and/or ingestion (Enyoh et al., 2020; Toussaint et al., 2019). The latter, through contamination of the food chain and drinking water, represents the major route of microplastic consumption by humans (Toussaint et al., 2019). It is commonly known that fish is the main contaminated food, but several recent published data show contamination in the whole food chain (Kosuth et al., 2018; Liebezeit and Liebezeit, 2013; Oliveri Conti et al., 2020; Yang et al., 2015). In addition, the worrying plastic levels in tap and spring water further confirm the estimation of 0.1–5 g average per week of microplastic ingestion in human body (Cox et al., 2019; Kosuth et al., 2018; Senathirajah et al., 2021).

Polystyrene is a thermoplastic polymer commonly used in food packaging. Like all plastics, polystyrene can be degraded into MPs and NPs by environmental agents and hence ingested. Although so far several works discussed the impact of MPs and NPs contamination on human health, there are no studies indicating a carcinogenic potential of polystyrene MPs and NPs. Here we show the potential human health cancer risk of MPs and NPs, by analyzing their impact on metabolism using an *in vitro* CCD-18Co normal human intestinal cell model in comparison to AOM (a potent carcinogenic agent) and HCT15 human colorectal cancer cell line. Using fluorescent NPs and MPs with 0.5 μm and 2 μm in diameter, respectively, we observed that NPs are more easily internalized after 48 h of exposure (Fig. 1) than MPs, which instead are gradually accumulated, reaching the same internalization level after 4 weeks (Fig. 4). On the other hand, NPs are released more easily than MPs when undergoing to intermittent exposure (Fig. 4). Furthermore, the quickly (NPs) and slowly (MPs) internalization occurs through both ATP-dependent and ATP-independent processes (Figure S1). Thus, NPs and MPs aggregation mechanisms (data not shown) could contribute to an overall increase in particles size and might affect their uptake and release (dos Santos et al., 2011; Fiorentino et al., 2015; Sousa de Almeida et al., 2021). Nonetheless, we did not observe neither cell mortality, nor cytotoxicity, nor immunogenic properties when tested on U-937 monocytes cell line (Figure S3). These results are consistent with published data by Weber and colleagues, where they state that spherical polystyrene particles do not significantly affect IL-6, TNF and IL-10 secretion in monocytes, as compared to control. Moreover, the same authors demonstrated that irregular polystyrene particles are able to induce a stronger release of pro-inflammatory cytokines, compared to spherical ones.

The increased ROS generation after 48 h of NPs exposure (Fig. 1) and under chronic NPs and MPs treatments for 4 weeks, as well as their decrease under intermittent exposure, indicate that it is dependent on the amount of internalized particles at this level of sizes (Fig. 4). These data are consistent with a previous report on mice treated with polystyrene particles showing accumulation in intestines, liver and kidneys inducing hepatic toxicity and oxidative stress (Deng et al., 2017). Moreover, we found that the redox stress effect on human cells after polystyrene particles internalization can be reversible, as previously observed in marine mussels (Huang et al., 2021).

Metabolomics profile, used to better characterize the effect of NPs and MPs on human colon cell metabolism, highlights the progressive impact of particles on glucose and glutamine metabolism, TCA cycle and oxidative stress between 48 h and 4 weeks of exposure similar to carcinogenic agents (Figs. 2, 3, 5 and 6). Metabolomics analysis performed after 48 h of exposure identifies an early metabolic rewiring showing increased level of glucose oxidation via lactate, glycolytic reserve and PPP (Figs. 3 and 4 and S1). These data, together with the not significant change in ATP synthesis and decreased levels of maximal respiration and spare respiratory capacity, highlight the role of glucose metabolic rewiring in sustaining energy metabolism under polystyrene exposure (Fig. 2). Canonical TCA cycle sustained by glucose and glutamine metabolism confirms that short NPs and MPs exposure does not influence energy metabolism (Figs. 2 and 3). This scenario is exacerbated after 4 weeks of exposure (Figs. 5 and 6). The significantly increased levels of glycolysis via lactate (Figs. 5C and 6A) and decreased levels of basal respiration and ATP production (Fig. 4E) show a metabolic shift in energy metabolism under MPs and NPs exposure. Exposure to MPs also induces increased levels of metabolites involved in PPP, Pro and GSH metabolism (Figs. 5 and 6) in response to oxidative stress in CCD-18Co cells (Fig. 5D). In addition, increased glutamine metabolism under MPs exposure and AOM treatments and in HCT15 tumor cells, confirmed by untargeted and targeted metabolic profiling, identifies the important role of this non-essential nutrient in metabolic shift (Bernfeld and Foster, 2019; Gaglio et al., 2020; Scalise et al., 2017; Tambay et al., 2021; Yuan et al., 2015). In particular, the increased levels of labeled metabolites, coming from [U-$^{13}C_5$]glutamine tracer, involved in TCA cycle both in forward and in reverse (through glutamine reductive carboxylation), highlights its role in anabolic processes usually observed in cancer (Metallo et al., 2011). The decoupling of glucose, used as energy source, and of glutamine, used to sustain anabolic process, is also a typical strategy of cancer cells to optimize nutrients utilization and to allow metabolic adaptation to environmental stress condition (Gaglio et al., 2011, 2020).

Therefore, in addition to other colon-rectal cancer risk factors, such as red meat or alcohol consumption (Bradbury et al., 2020), our results contribute to demonstrate the key role of nutrition and of a healthy food chain to reduce risk of specific cancers.

5. Conclusions

In conclusion, our results show that polystyrene micro and nanoparticles can be internalized in human colon cells and can induce metabolic changes under acute and chronic exposure.

Normal human colon cell line after exposure to polystyrene particles shows a rearrangement of normal metabolic pathways similar to carcinogenic agent AOM treatment and HCT15 colon cancer cells. Specifically, these cells show simultaneously four metabolic cancer hallmarks: i) increased glucose oxidation via lactate even when oxygen is available, ii) reduced activity of mitochondria, iii) decoupling of nutrients (glucose and glutamine) and iv) reductive carboxylation of glutamine (Hanahan et al., 2000; Gaglio et al., 2011; Metallo et al., 2011).

Therefore, the metabolic rewiring in plastics-treated cells is the experimental evidence that chronic polystyrene exposure could act as a cancer risk factor for human health.

Credit author statement

Marcella Bonanomi: Methodology, Validation, Visualization and Formal analysis. Noemi Salmistraro: Validation and Visualization. Annalisa Pinsino: starting conceptual idea. Anna Maria Colangelo: Writing – original draft. Danilo Porro: Writing – original draft. Daniela Gaglio: Conceptualization, Methodology, Data curation, Formal analysis, Software, Visualization, Writing – original draft, Supervision, Project administration. All authors have read and agreed to the published version of the manuscript.

Funding

This research did not receive any specific grant from funding agencies in the public, commercial, or not-for-profit sectors.

Institutional review board statement

Not applicable.

Informed consent statement

Not applicable.

Declaration of competing interest

The authors declare that they have no known competing financial interests or personal relationships that could have appeared to influence the work reported in this paper.

Appendix A. Supplementary data

Supplementary data to this article can be found online at https://doi.org/10.1016/j.chemosphere.2022.134947.

References

Al-Numair, K.S., Chandramohan, G., Alsaif, M.A., 2012. Pretreatment with morin, a flavonoid, ameliorates adenosine triphosphatases and glycoproteins in isoproterenol-induced myocardial infarction in rats. J. Nat. Med. 66, 95–101. https://doi.org/10.1007/s11418-011-0558-2.

Andrady, A.L., Neal, M.A., 2009. Applications and societal benefits of plastics. Phil. Trans. Biol. Sci. 364, 1977–1984. https://doi.org/10.1098/rstb.2008.0304.

Antoniewicz, M.R., 2018. A guide to 13C metabolic flux analysis for the cancer biologist. Exp. Mol. Med. 50, 19. https://doi.org/10.1038/s12276-018-0060-y.

Bernfeld, E., Foster, D.A., 2019. Glutamine as an essential amino acid for KRas-driven cancer cells. Trends Endocrinol. Metabol. 30, 357–368. https://doi.org/10.1016/j.tem.2019.03.003.

Bonanomi, M., Salmistraro, N., Fiscon, G., Conte, F., Paci, P., Bravatà, V., Forte, G.I., Volpari, T., Scorza, M., Mastroianni, F., D'Errico, S., Avolio, E., Piccialli, G., Colangelo, A.M., Vanoni, M., Gaglio, D., Alberghina, L., 2021. Transcriptomics and metabolomics integration reveals redox-dependent metabolic rewiring in breast cancer cells. Cancers 13, 5058. https://doi.org/10.3390/cancers13205058.

Bradbury, K.E., Murphy, N., Key, T.J., 2020. Diet and colorectal cancer in UK Biobank: a prospective study. Int. J. Epidemiol. 49, 246–258. https://doi.org/10.1093/ije/dyz064.

Chang, X., Xue, Y., Li, J., Zou, L., Tang, M., 2020. Potential health impact of environmental micro- and nanoplastics pollution. J. Appl. Toxicol. 40, 4–15. https://doi.org/10.1002/jat.3915.

Cox, K.D., Covernton, G.A., Davies, H.L., Dower, J.F., Juanes, F., Dudas, S.E., 2019. Human consumption of microplastics. Environ. Sci. Technol. 53, 7068–7074. https://doi.org/10.1021/acs.est.9b01517.

da Costa, J.P., Santos, P.S.M., Duarte, A.C., Rocha-Santos, T., 2016. Nano)plastics in the environment – sources, fates and effects. Sci. Total Environ. 566–567, 15–26. https://doi.org/10.1016/j.scitotenv.2016.05.041.

Danopoulos, E., Twiddy, M., West, R., Rotchell, J.M., 2022. A rapid review and meta-regression analyses of the toxicological impacts of microplastic exposure in human cells. J. Hazard Mater. 427, 127861. https://doi.org/10.1016/j.jhazmat.2021.127861.

Deng, Y., Zhang, Y., Lemos, B., Ren, H., 2017. Tissue accumulation of microplastics in mice and biomarker responses suggest widespread health risks of exposure. Sci. Rep. 7, 46687. https://doi.org/10.1038/srep46687.

dos Santos, T., Varela, J., Lynch, I., Salvati, A., Dawson, K.A., 2011. Effects of transport inhibitors on the cellular uptake of carboxylated polystyrene nanoparticles in different cell lines. PLoS One 6, e24438. https://doi.org/10.1371/journal.pone.0024438.

Enyoh, C.E., Shafea, L., Verla, A.W., Verla, E.N., Qingyue, W., Chowdhury, T., Paredes, M., 2020. Microplastics exposure routes and toxicity studies to ecosystems: an overview. Environ. Anal. Health Toxicol. 35 https://doi.org/10.5620/eaht.e2020004.

Fackelmann, G., Sommer, S., 2019. Microplastics and the gut microbiome: how chronically exposed species may suffer from gut dysbiosis. Mar. Pollut. Bull. 143, 193–203. https://doi.org/10.1016/j.marpolbul.2019.04.030.

Fiorentino, I., Gualtieri, R., Barbato, V., Mollo, V., Braun, S., Angrisani, A., Turano, M., Furia, M., Netti, P.A., Guarnieri, D., Fusco, S., Talevi, R., 2015. Energy independent uptake and release of polystyrene nanoparticles in primary mammalian cell cultures. Exp. Cell Res. 330, 240–247. https://doi.org/10.1016/j.yexcr.2014.09.017.

Gaglio, D., Bonanomi, M., Valtorta, S., Bharat, R., Ripamonti, M., Conte, F., Fiscon, G., Righi, N., Napodano, E., Papa, F., Raccagni, I., Parker, S.J., Cifola, I., Camboni, T., Paci, P., Colangelo, A.M., Vanoni, M., Metallo, C.M., Moresco, R.M., Alberghina, L., 2020. Disruption of redox homeostasis for combinatorial drug efficacy in K-Ras tumors as revealed by metabolic connectivity profiling. Cancer Metabol. 8, 22. https://doi.org/10.1186/s40170-020-00227-4.

Gaglio, D., Metallo, C.M., Gameiro, P.A., Hiller, K., Danna, L.S., Balestrieri, C., Alberghina, L., Stephanopoulos, G., Chiaradonna, F., 2011. Oncogenic K-Ras decouples glucose and glutamine metabolism to support cancer cell growth. Mol. Syst. Biol. 7, 523. https://doi.org/10.1038/msb.2011.56.

Gaglio, D., Valtorta, S., Ripamonti, M., Bonanomi, M., Damiani, C., Todde, S., Negri, A.S., Sanvito, F., Mastroianni, F., Campli, A.D., Turacchio, G., Grigoli, G.D., Belloli, S., Luini, A., Gilardi, M.C., Colangelo, A.M., Alberghina, L., Moresco, R.M., 2016. Divergent in vitro/in vivo responses to drug treatments of highly aggressive NIH-Ras cancer cells: a PET imaging and metabolomics-mass-spectrometry study. Oncotarget 7, 52017–52031. https://doi.org/10.18632/oncotarget.10470.

Gigault, J., Halle, A. ter, Baudrimont, M., Pascal, P.-Y., Gauffre, F., Phi, T.-L., El Hadri, H., Grassl, B., Reynaud, S., 2018. Current opinion: what is a nanoplastic? Environ. Pollut. 235, 1030–1034. https://doi.org/10.1016/j.envpol.2018.01.024.

Groh, K.J., Backhaus, T., Carney-Almroth, B., Geueke, B., Inostroza, P.A., Lennquist, A., Leslie, H.A., Maffini, M., Slunge, D., Trasande, L., Warhurst, A.M., Muncke, J., 2019. Overview of known plastic packaging-associated chemicals and their hazards. Sci. Total Environ. 651, 3253–3268. https://doi.org/10.1016/j.scitotenv.2018.10.015.

Hanahan, D., Weinberg, R.A., 2000. The hallmarks of cancer. Cell 100, 57–70. https://doi.org/10.1016/s0092-8674(00)81683-9.

Huang, W., Song, B., Liang, J., Niu, Q., Zeng, G., Shen, M., Deng, J., Luo, Y., Wen, X., Zhang, Y., 2021. Microplastics and associated contaminants in the aquatic environment: a review on their ecotoxicological effects, trophic transfer, and potential impacts to human health. J. Hazard Mater. 405, 124187. https://doi.org/10.1016/j.jhazmat.2020.124187.

Huerta Lwanga, E., Mendoza Vega, J., Ku Quej, V., Chi, J. de los A., Sanchez del Cid, L., Chi, C., Escalona Segura, G., Gertsen, H., Salánki, T., van der Ploeg, M., Koelmans, A. A., Geissen, V., 2017. Field evidence for transfer of plastic debris along a terrestrial food chain. Sci. Rep. 7, 14071. https://doi.org/10.1038/s41598-017-14588-2.

Jans, J.J.M., Broeks, M.H., Verhoeven-Duif, N.M., 2022. Metabolomics in diagnostics of inborn metabolic disorders. Curr. Opin. Struct. Biol. 29, 100409. https://doi.org/10.1016/j.coisb.2021.100409.

Jiang, B., Kauffman, A.E., Li, L., McFee, W., Cai, B., Weinstein, J., Lead, J.R., Chatterjee, S., Scott, G.I., Xiao, S., 2020. Health impacts of environmental contamination of micro- and nanoplastics: a review. Environ. Health Prev. Med. 25, 29. https://doi.org/10.1186/s12199-020-00870-9.

Kik, K., Bukowska, B., Sicińska, P., 2020. Polystyrene nanoparticles: sources, occurrence in the environment, distribution in tissues, accumulation and toxicity to various organisms. Environ. Pollut. 262, 114297. https://doi.org/10.1016/j.envpol.2020.114297.

Kosuth, M., Mason, S.A., Wattenberg, E.V., 2018. Anthropogenic contamination of tap water, beer, and sea salt. PLoS One 13, e0194970. https://doi.org/10.1371/journal.pone.0194970.

Krzywinski, M., Schein, J., Birol, I., Connors, J., Gascoyne, R., Horsman, D., Jones, S.J., Marra, M.A., 2009. Circos: an information aesthetic for comparative genomics. Genome Res. 19, 1639–1645. https://doi.org/10.1101/gr.092759.109.

Lambert, S., Wagner, M., 2016. Characterisation of nanoplastics during the degradation of polystyrene. Chemosphere 145, 265–268. https://doi.org/10.1016/j.chemosphere.2015.11.078.

Lehner, R., Weder, C., Petri-Fink, A., Rothen-Rutishauser, B., 2019. Emergence of nanoplastic in the environment and possible impact on human health. Environ. Sci. Technol. 53, 1748–1765. https://doi.org/10.1021/acs.est.8b05512.

Lei, K., Qiao, F., Liu, Q., Wei, Z., Qi, H., Cui, S., Yue, X., Deng, Y., An, L., 2017. Microplastics releasing from personal care and cosmetic products in China. Mar. Pollut. Bull. 123, 122–126. https://doi.org/10.1016/j.marpolbul.2017.09.016.

Leslie, H.A., van Velzen, M.J.M., Brandsma, S.H., Vethaak, A.D., Garcia-Vallejo, J.J., Lamoree, M.H., 2022. Discovery and quantification of plastic particle pollution in human blood. Environ. Int. 163, 107199. https://doi.org/10.1016/j.envint.2022.107199.

Li, B., Ding, Y., Cheng, X., Sheng, D., Xu, Z., Rong, Q., Wu, Y., Zhao, H., Ji, X., Zhang, Y., 2020. Polyethylene microplastics affect the distribution of gut microbiota and inflammation development in mice. Chemosphere 244, 125492. https://doi.org/10.1016/j.chemosphere.2019.125492.

Li, J., Yang, D., Li, L., Jabeen, K., Shi, H., 2015. Microplastics in commercial bivalves from China. Environ. Pollut. 207, 190–195. https://doi.org/10.1016/j.envpol.2015.09.018.

Liebezeit, G., Liebezeit, E., 2013. Non-pollen particulates in honey and sugar. Food Addit. Contam. Part A Chem Anal Control Expo Risk Assess 30, 2136–2140. https://doi.org/10.1080/19440049.2013.843025.

Lim, S.L., Ng, C.T., Zou, L., Lu, Y., Chen, J., Bay, B.H., Shen, H.-M., Ong, C.N., 2019. Targeted metabolomics reveals differential biological effects of nanoplastics and nanoZnO in human lung cells. Nanotoxicology 13, 1117–1132. https://doi.org/10.1080/17435390.2019.1640913.

Liu, L., Xu, K., Zhang, B., Ye, Y., Zhang, Q., Jiang, W., 2021. Cellular internalization and release of polystyrene microplastics and nanoplastics. Sci. Total Environ. 779, 146523. https://doi.org/10.1016/j.scitotenv.2021.146523.

Liu, Y., Wang, Z., Zhang, Q., Bai, H., Cai, Y., Yan, Z., Lv, Q., 2019. Optimization of multi-residue method for targeted screening and quantification of 216 harmful chemicals in plastic children's toys by gas chromatography-tandem mass spectrometry analysis. J. Chromatogr. A 1603, 311–326. https://doi.org/10.1016/j.chroma.2019.06.047.

Marsh, K., Bugusu, B., 2007. Food packaging–roles, materials, and environmental issues. J. Food Sci. 72, R39–R55. https://doi.org/10.1111/j.1750-3841.2007.00301.x.

Mason, S.A., Welch, V.G., Neratko, J., 2018. Synthetic polymer contamination in bottled water. Front. Chem. 6, 407. https://doi.org/10.3389/fchem.2018.00407.

Metallo, C.M., Gameiro, P.A., Bell, E.L., Mattaini, K.R., Yang, J., Hiller, K., Jewell, C.M., Johnson, Z.R., Irvine, D.J., Guarente, L., Kelleher, J.K., Vander Heiden, M.G., Iliopoulos, O., Stephanopoulos, G., 2011. Reductive glutamine metabolism by IDH1 mediates lipogenesis under hypoxia. Nature 481, 380–384. https://doi.org/10.1038/nature10602.

Neves, D., Sobral, P., Ferreira, J.L., Pereira, T., 2015a. Ingestion of microplastics by commercial fish off the Portuguese coast. Mar. Pollut. Bull. 101, 119–126. https://doi.org/10.1016/j.marpolbul.2015.11.008.

Neves, D., Sobral, P., Pereira, T., 2015b. Marine litter in bottom trawls off the Portuguese coast. Mar. Pollut. Bull. 99, 301–304. https://doi.org/10.1016/j.marpolbul.2015.07.044.

Oliveri Conti, G., Ferrante, M., Banni, M., Favara, C., Nicolosi, I., Cristaldi, A., Fiore, M., Zuccarello, P., 2020. Micro- and nano-plastics in edible fruit and vegetables. The first diet risks assessment for the general population. Environ. Res. 187, 109677. https://doi.org/10.1016/j.envres.2020.109677.

Qiao, R., Sheng, C., Lu, Y., Zhang, Y., Ren, H., Lemos, B., 2019. Microplastics induce intestinal inflammation, oxidative stress, and disorders of metabolome and microbiome in zebrafish. Sci. Total Environ. 662, 246–253. https://doi.org/10.1016/j.scitotenv.2019.01.245.

Ragusa, A., Svelato, A., Santacroce, C., Catalano, P., Notarstefano, V., Carnevali, O., Papa, F., Rongioletti, M.C.A., Baiocco, F., Draghi, S., D'Amore, E., Rinaldo, D., Matta, M., Giorgini, E., 2021. Plasticenta: first evidence of microplastics in human placenta. Environ. Int. 146, 106274. https://doi.org/10.1016/j.envint.2020.106274.

Ribeiro, F., Okoffo, E.D., O'Brien, J.W., Fraissinet-Tachet, S., O'Brien, S., Gallen, M., Samanipour, S., Kaserzon, S., Mueller, J.F., Galloway, T., Thomas, K.V., 2020. Quantitative analysis of selected plastics in high-commercial-value Australian seafood by pyrolysis gas chromatography mass spectrometry. Environ. Sci. Technol. 54, 9408–9417. https://doi.org/10.1021/acs.est.0c02337.

Scalise, M., Pochini, L., Galluccio, M., Console, L., Indiveri, C., 2017. Glutamine transport and mitochondrial metabolism in cancer cell growth. Front. Oncol. 7, 306. https://doi.org/10.3389/fonc.2017.00306.

Schymanski, D., Goldbeck, C., Humpf, H.-U., Fürst, P., 2018. Analysis of microplastics in water by micro-Raman spectroscopy: release of plastic particles from different packaging into mineral water. Water Res. 129, 154–162. https://doi.org/10.1016/j.watres.2017.11.011.

Senathirajah, K., Attwood, S., Bhagwat, G., Carbery, M., Wilson, S., Palanisami, T., 2021. Estimation of the mass of microplastics ingested - a pivotal first step towards human health risk assessment. J. Hazard Mater. 404, 124004. https://doi.org/10.1016/j.jhazmat.2020.124004.

Sousa de Almeida, M., Susnik, E., Drasler, B., Taladriz-Blanco, P., Petri-Fink, A., Rothen-Rutishauser, B., 2021. Understanding nanoparticle endocytosis to improve targeting strategies in nanomedicine. Chem. Soc. Rev. 50, 5397–5434. https://doi.org/10.1039/d0cs01127d.

Sullivan, L.B., Gui, D.Y., Vander Heiden, M.G., 2016. Altered metabolite levels in cancer: implications for tumour biology and cancer therapy. Nat. Rev. Cancer 16, 680–693. https://doi.org/10.1038/nrc.2016.85.

Tambay, V., Raymond, V.-A., Bilodeau, M., 2021. MYC rules: leading glutamine metabolism toward a distinct cancer cell phenotype. Cancers 13, 4484. https://doi.org/10.3390/cancers13174484.

Thompson, R.C., Moore, C.J., vom Saal, F.S., Swan, S.H., 2009. Plastics, the environment and human health: current consensus and future trends. Philos. Trans. R. Soc. Lond. B Biol. Sci. 364, 2153–2166. https://doi.org/10.1098/rstb.2009.0053.

Toussaint, B., Raffael, B., Angers-Loustau, A., Gilliland, D., Kestens, V., Petrillo, M., Rio-Echevarria, I.M., Van den Eede, G., 2019. Review of micro- and nanoplastic contamination in the food chain. Food Addit. Contam. Part A Chem Anal Control Expo Risk Assess 36, 639–673. https://doi.org/10.1080/19440049.2019.1583381.

van Wijnen, J., Ragas, A.M.J., Kroeze, C., 2019. Modelling global river export of microplastics to the marine environment: sources and future trends. Sci. Total Environ. 673, 392–401. https://doi.org/10.1016/j.scitotenv.2019.04.078.

Waly, M.A., Abou-Zeid, L., El-Gogary, S.R., Shalaby, M.A., 2012. One-pot synthesis, molecular modeling and in vitro antibacterial activity of novel 3-(1,3,4-Oxadiazol-2-yl) Quinoxaline 1,4-dioxide and pyrazolyl analogs. Acta Chim. Slov. 59, 32–41.

Wang, Q., Bai, J., Ning, B., Fan, L., Sun, T., Fang, Y., Wu, J., Li, S., Duan, C., Zhang, Y., Liang, J., Gao, Z., 2020. Effects of bisphenol A and nanoscale and microscale polystyrene plastic exposure on particle uptake and toxicity in human Caco-2 cells. Chemosphere 254, 126788. https://doi.org/10.1016/j.chemosphere.2020.126788.

Weber, A., Schwiebs, A., Solhaug, H., Stenvik, J., Nilsen, A.M., Wagner, M., Relja, B., Radeke, H.H., 2022. Nanoplastics affect the inflammatory cytokine release by primary human monocytes and dendritic cells. Environ. Int. 163, 107173. https://doi.org/10.1016/j.envint.2022.107173.

Wu, B., Wu, X., Liu, S., Wang, Z., Chen, L., 2019. Size-dependent effects of polystyrene microplastics on cytotoxicity and efflux pump inhibition in human Caco-2 cells. Chemosphere 221, 333–341. https://doi.org/10.1016/j.chemosphere.2019.01.056.

Yang, D., Shi, H., Li, L., Li, J., Jabeen, K., Kolandhasamy, P., 2015. Microplastic pollution in table salts from China. Environ. Sci. Technol. 49, 13622–13627. https://doi.org/10.1021/acs.est.5b03163.

Yee, M.S.-L., Hii, L.-W., Looi, C.K., Lim, W.-M., Wong, S.-F., Kok, Y.-Y., Tan, B.-K., Wong, C.-Y., Leong, C.-O., 2021. Impact of microplastics and nanoplastics on human health. Nanomaterials 11, 496. https://doi.org/10.3390/nano11020496.

Yong, C.Q.Y., Valiyaveettil, S., Tang, B.L., 2020. Toxicity of microplastics and nanoplastics in mammalian systems. Int. J. Environ. Res. Publ. Health 17, E1509. https://doi.org/10.3390/ijerph17051509.

Yuan, L., Sheng, X., Willson, A.K., Roque, D.R., Stine, J.E., Guo, H., Jones, H.M., Zhou, C., Bae-Jump, V.L., 2015. Glutamine promotes ovarian cancer cell proliferation through the mTOR/S6 pathway. Endocr. Relat. Cancer 22, 577–591. https://doi.org/10.1530/ERC-15-0192.

Zarus, G.M., Muianga, C., Hunter, C.M., Pappas, R.S., 2021. A review of data for quantifying human exposures to micro and nanoplastics and potential health risks. Sci. Total Environ. 756, 144010. https://doi.org/10.1016/j.scitotenv.2020.144010.